PHYSICAL REVIEW A VOLUME 3, NUMBER 1 JANUARY 1971

Determination of Energies and Lifetimes of the Metastable Auto-Ionizing $(1s2s2p)\,^4P$ States of Li^6 and Li^7 by a Zeeman-Quenching Technique*

M. Levitt and R. Novick
Columbia Radiation Laboratory, Department of Physics, Columbia University, New York, New York 10027

and

P. D. Feldman†
The Johns Hopkins University, Department of Physics, Baltimore, Maryland 21218
(Received 14 July 1970)

A Zeeman-quenching atomic-beam method has been utilized for the determination of the fine- and hyperfine-structure energies and auto-ionization lifetimes of the metastable $(1s2s2p)\,^4P_J$ states of Li^6 and Li^7. Both the fine-structure intervals and the lifetimes of the $J=\frac{3}{2}$ and $J=\frac{1}{2}$ states are found to be in disagreement with existing theoretical calculations. The quenching of metastable lithium atoms in a nonuniform magnetic field can be satisfactorily described with the aid of the "adiabatic criterion." The present results also permit a quantitative evaluation of a proposal for producing polarized lithium nuclei.

I. INTRODUCTION

One of the most important properties of the metastable auto-ionizing atomic states discovered by Feldman and Novick[1] (FN) is the differential metastability of the fine- and hyperfine-structure levels. This property results from the difference in the degree of coupling to the continuum of each of these states. The effect of a magnetic field is to mix the magnetic substates of the longer-lived levels with those of the shorter-lived ones causing a resultant decrease in the apparent lifetime of the former. This "Zeeman quenching" of an atomic beam of metastable auto-ionizing atoms has been observed in lithium,[2] potassium, and rubidium.[3]

From an analysis of field-dependent structure (due to anticrossings of magnetic substates) in the quenching functions of Li^7 and Li^6, it was possible to make precise determination of the fine structure of the $(1s2s2p)\,^4P$ state and to determine the relative lifetimes of the three different J levels.[4] The energy intervals were verified by the subsequent identification[5] of two multiplets in the optical spectrum[6] of Li^7 which result from transitions between certain doubly excited states[7] and the $(1s2s2p)\,^4P$ levels.

The Zeeman-quenching effect has also been used as the basis for state selection and analysis in a microwave atomic-beam resonance experiment of Novick and Sprott[8] on the quartet metastable level of potassium. By observing the magnetic-field dependence of the energy splitting between various hyperfine levels, they were able to determine the configuration, term assignment, and hyperfine energy constants of the metastable auto-ionizing states at 19.9 eV.

In the present paper, we describe in detail the Zeeman-quenching experiments and the analysis of the fine and hyperfine structure of the metastable states of Li^6 and Li^7. For Li^7, the appreciable mixing of fine-structure states by the hyperfine interactions even in the absence of a magnetic field requires an increase of about 15% in the value reported by FN for the lifetime of the $(1s2s2p)\,^4P_{5/2}$ state. The corrected experimental lifetime, (5.8 ± 1.2) μsec, is in better agreement with the theoretical value 5.88 μsec calculated by Manson.[9] It is also shown that observations of the quenching of metastable atoms as they pass across the pole tips of a cylindrical magnet can be fully understood if the adiabatic criterion[10] is used to determine whether or not transitions occur in the fringing fields. However, in order to optimize the agreement with the data, bombardment polarization effects must be included in the theoretical analysis. Finally, we present the results of calculations of the vector and tensor nuclear polarizations obtainable in Li^6 $(I=1)$ by means of Zeeman quenching, and we discuss a possible radio-frequency method for obtaining enhanced polarization.

II. METASTABLE $(1s2s2p)\,^4P$ STATE OF LITHIUM

The states with which we are concerned here are quartets which arise from excitation of an inner-shell electron of lithium. These quartet states are metastable even though they lie well above the lithium ionization limit, because they are bound with respect to the first triplet excited state of Li^+. They are thus degenerate with the doublet but not with the quartet continuum and do not satisfy the $\Delta S = 0$ selection rule for auto-ionization via the Coulomb interaction. In FN, it is shown that the transition to the continuum can proceed only via the magnetic interactions between electrons. Radiative decay is

also forbidden.

Since the auto-ionization decay results from the fine-structure interactions, the various fine-structure (fs) levels having different symmetry will couple differently to the continuum. For example, consider the three J levels ($^4P_{5/2}$, $^4P_{3/2}$, $^4P_{1/2}$) of the ($1s2s2p$) configuration of Li [ignoring hyperfine structure (hfs)]. The $^4P_{3/2}$ and $^4P_{1/2}$ states are coupled to continuum [$^1S_0(\mathrm{Li}^+) + k^2 p_{3/2,\,1/2}$] states through the spin-orbit, spin-other-orbit, and spin-spin interactions. In addition, these same states are coupled to the continuum in second order through the rapidly auto-ionizing ($1s2s2p$) $^2P_{3/2,\,1/2}$ states by the same magnetic interactions. The state of highest total angular momentum $^4P_{5/2}$ is necessarily a pure-quartet level and is coupled to the continuum [$^1S_0(\mathrm{Li}^+) + k^2 f_{5/2}$] state only by the tensor part of the spin-spin interaction. Thus, if all of the matrix elements are comparable in magnitude, it is expected that the decay rate for this state would be smaller than that for either the $^4P_{3/2}$ or $^4P_{1/2}$ states. Detailed calculations of the auto-ionization rates by several authors[11,12] yield results which are in agreement with these qualitative arguments.

We must also consider the effect of hyperfine structure in the case of Li^7, since the Fermi-contact interaction for the unpaired core $1s$ electron is comparable to the fine-structure splitting of the ^4P_J levels. The large magnetic dipole hyperfine interaction strongly mixes fine-structure levels with J differing by 1. The quadrupole interaction, which is about three orders of magnitude smaller than the magnetic dipole term, couples fine-structure levels differing in J by 1 and 2. The effect of the hyperfine mixing is to produce states of total angular momentum $\vec{F}$ ($\vec{F} = \vec{I} + \vec{J}$) with different lifetimes. The state of highest total angular momentum ($F = 4$ in the case of Li^7) will have the lifetime of the pure ($1s2s2p$) $^4P_{5/2}$ state. Levels of lower total angular momenta will have lifetimes intermediate between those of the pure $^4P_{5/2}$, $^4P_{3/2}$, and $^4P_{1/2}$ levels depending upon the degree of mixing. In general, those hyperfine states with large $^4P_{5/2}$ components will be longer-lived than those with large $^4P_{3/2}$ and $^4P_{1/2}$ amplitudes.

The case of interest to us occurs when the Zeeman energy for a given magnetic field is comparable to the fs and hfs energies (which are of order 1 cm^{-1}). This results in additional mixing between substates according to the selection rules $\Delta M_F = 0$, $\Delta F = 0, \pm 1$. The auto-ionization decay rates of a group of states degenerate at zero field will then depend upon the strength of the magnetic field and on the magnetic quantum number M_F characterizing the group. Since the energy of a magnetic moment having a strength of 1 μ_B in a field of 10 kG is 0.467 cm^{-1}, we expect significant mixing in magnetic fields that are readily available in the laboratory. The $^4P_{5/2}$ states with $F = 4$ and $M_F = \pm 4$ will remain "pure" and couple to the continuum only through the spin-spin interaction even when hfs and Zeeman mixing are included. The other hyperfine components of $^4P_{5/2}$ couple to the continuum in a magnetic-field–dependent manner, and the application of an external field to a beam of atoms in the metastable states will alter the lifetime of these atoms.

At this point, it is of interest to examine the possibility of observing Zeeman quenching in atomic states which are metastable against radiative decay.[13] Consider, for example, the elements for which the lowest excited ^3P level lies below the first ^3S level, e.g., Ne, Ar, Zn, Cd, and Hg. The $^3P_1$ state can decay by emitting an intercombination line, since it is mixed by the fs interaction with $^1P_1$, but $^3P_{0,2}$ are pure triplet states and hence are metastable. The application of an external magnetic field will mix the states $^3P_{0,2}$ with $^3P_1$ so that the former states will in principle be somewhat quenched. We can estimate the magnitude of the field required for appreciable quenching by using perturbation theory to estimate the metastable-state decay rate as a function of magnetic field:

$$\gamma_L(H) \approx \gamma_S(0)\,[\mu_B H/(E_L - E_S)]^2, \qquad (1)$$

where subscripts L and S refer to the longer- and shorter-lived states, respectively; E is the state energy; μ_B is the Bohr magneton, and H is the magnetic-field strength. For the Zn, Cd, and Hg group, the quantity $\gamma_S/(\Delta E)^2$ does not vary greatly, enabling us to obtain the approximate numerical expression

$$\gamma_L(H) \approx 3\times 10^{-3} H^2 \ \mathrm{sec}^{-1}, \qquad (2)$$

where H is in kG.

Thus, fields of the order of 10^6 G or higher are needed to produce observable lines originating in the $^3P_2$ and $^3P_0$ levels of these elements. By comparison, the factor $\gamma_S/(\Delta E)^2$ in Eq. (1) is much larger for the metastable quartet states of lithium, with the result that significant quenching can be obtained with magnetic fields readily available in the laboratory. It is noteworthy that the hyperfine fields in Hg are sufficient to produce observable forbidden lines ($^3P_0$, λ2656; $^3P_2$, λ 2270).[14]

III. EXPERIMENTAL ARRANGEMENT

The first experimental arrangement used to study the quenching effect is shown in Fig. 1. Except for the quenching magnet placed between the source and the detector, the apparatus was the same as that described in FN. The effective length of the field was 1 cm, and the gap spacing was 0.5 mm. A maximum field of 19 kG was obtained with Permendur pole tips and a current of 50 A in the water-cooled windings. Calibration of the magnetic field,

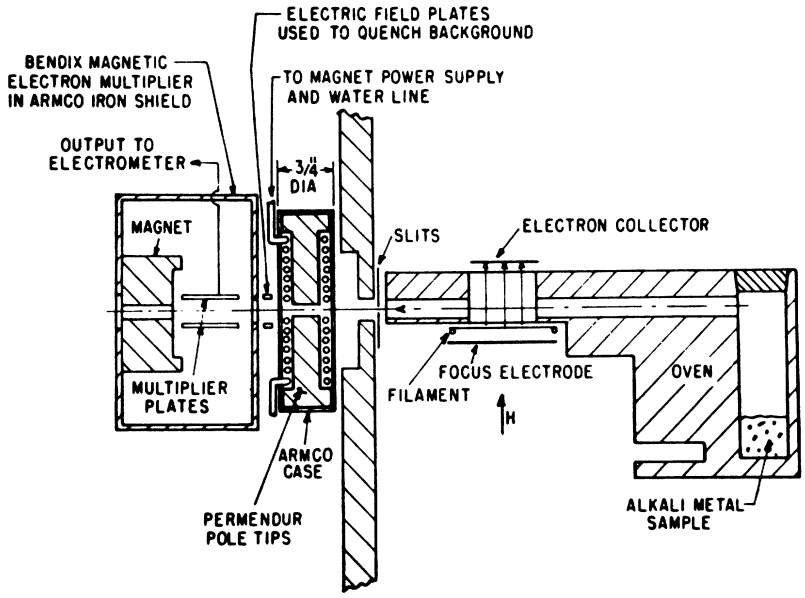

FIG. 1 Schematic diagram of the first Zeeman-quenching atomic-beam apparatus.

accomplished with the aid of an F.W. Bell model 120 gaussmeter and a 0.4-mm Hall probe, was reproducible to a few percent. The detector used in these experiments was a modified Bendix 306 magnetic electron multiplier mounted in a magnetic shield of Armco iron and is described in FN.

The Armco shield on the detector prevented the multiplier gain from being affected by leakage fields from the quenching magnet. In practice, the electron-bombarding energy was modulated at 280 Hz, and the amplified output from the multiplier was directed to a phase-sensitive detector synchronized to the modulating frequency. Data points were obtained by comparing the multiplier output at a given value of the quenching field to the signal at zero field. The results for Li^6 and Li^7 are shown in Fig. 2. It can be seen that there are several resonancelike dips and at least one field region where the Li^7 signal decreases markedly with increasing field but does not correspondingly increase at still higher fields. Since it was thought that the structure of the observed "line shapes" might result from nonadiabatic transitions arising from the passage of metastables through the field gradients at the edges of the quenching magnet, the experiment was redesigned to eliminate any such effects.

In the second apparatus, the entire experiment, including production and detection of the metastable atoms, was done in a uniform magnetic field. The vacuum envelope, aside from pumping and electrical-feedthrough ports, was a pancake-shaped copper chamber, with 8 in. diam by 2 in. width which was situated between the 12-in.-diam soft-iron pole pieces of a Harvey-Wells model L-128 electromagnet. A block diagram of the basic experimental configuration is shown in Fig. 3.

The neutral atomic beam energed from a $\frac{1}{8}$-in.-diam canal in a molybdenum oven, and was bombarded by an electron beam produced by a regulated triode electron gun. The detector consisted of a grounded copper box containing a system of grids to accelerate electrons from decaying metastable atoms to a Faraday collector. Collimation at the entrance to the detector was originally provided by two molybdenum plates maintained at a potential difference of about 500 V, which served to collect stray charged particles. In order to move the detector closer to the oven and thereby increase the signal, the plates were replaced by a collimating slit $\frac{3}{16}$ in. wide by $\frac{1}{16}$ in. high and $\frac{1}{8}$ in. long, placed in a previously unoccupied region between the detector and oven. This restricted the operating fields to values greater than 5 kG to avoid an excessive charged-particle background.

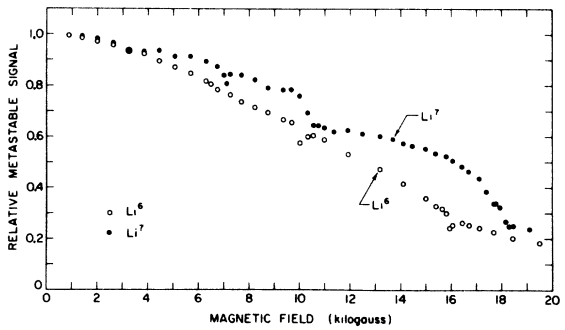

FIG. 2. Zeeman-quenching data for Li^6 and Li^7 obtained with the apparatus of Fig. 1.

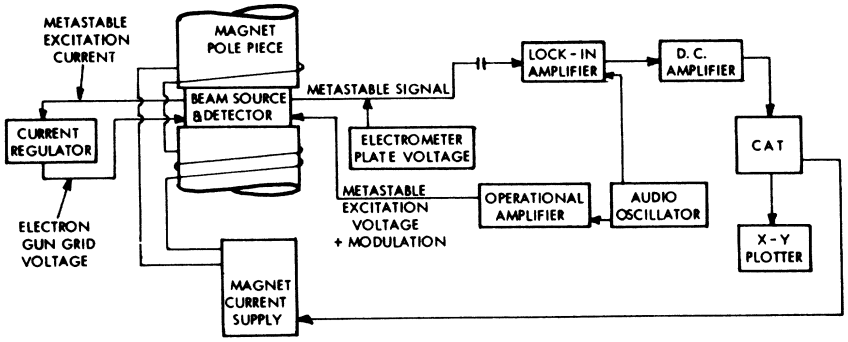

FIG. 3. Schematic diagram of the components of the uniform-field quenching experiment.

After passing through a slit in the grounded detector box, the beam entered a smaller copper box which was maintained at a potential of − 135 V. One of the two sides of this box which was parallel to the pole pieces was open, and the face opposite the open side was covered with a plate made of platinum, which has a relatively high work function of ≈ 5. 5 eV. This arrangement was used so that photons produced in the electron-bombardment region would have a low probability of producing photoelectrons in the detector. Electrons from decaying metastables were then accelerated along the magnetic field through two grids to a collecting plate arranged in such a way as to minimize secondary electron emission from the collector. The current at the collector (typically ~ 10^{-13} A) was measured with a magnetically shielded electrometer.

The electrometer output was amplified and synchronously rectified by a phase-sensitive amplifier locked to the electron-beam modulation frequency. For qualitative measurements of Zeeman quenching, the signal output from the amplifier was applied to a Varian 10-mV chart recorder. Magnetic-field measurements were made with a small rotating coil, placed in the field, which generated a 30-Hz sine wave whose amplitude was proportional to the field strength. The 30-Hz signal was rectified and amplified, and the dc level, measured with a Vidar-500 digital voltmeter, was calibrated against a proton NMR signal.

It was found that by using a lock-in time constant of 10 sec, the experimental signal-to-noise ratio associated with the signal from the sum of all long-lived states was about 100:1. However, for precise determinations of the anticrossing line shapes, which result from a change in the decay probability of only one of the long-lived states, an increase in the signal-to-noise ratio was necessary. To achieve this, the phase-locked amplifier output was further amplified to a level of about 1 V and fed into a 400-channel TMC CAT 400-B digital signal averager, which stored and averaged the signal pattern from a number of successive sweeps over a given magnetic-field region of interest.

In using the signal averager, the correspondence between channel number and magnetic-field value was maintained by injecting an analog voltage proportional to the channel number from the CAT into the sweep input of the magnet current supply. An Alpha Scientific NMR probe was used with a mineral-oil sample to obtain H in terms of proton NMR frequencies. The relationship between field value and channel number was determined by stopping the field sweep at several discrete positions and measuring the proton NMR frequency. The field values corresponding to other channels were obtained by linear interpolation between the selected channels. Since the calibration data were obtained under static conditions, the interpolated values of magnetic field had to be corrected for phase delays that arise when the field is varied continuously. In no case is this correction larger than 1. 25 G. There is also a 0. 25-G correction to compensate for the difference in field strength between the atomic-beam path and the position of the NMR probe. Spatial variation of the field over the path length of the beam and short-term fluctuations in the magnet current produce a broadening of the line shapes estimated at ≈ 0. 5 G.

IV. OBSERVATIONS

Using the uniform-field apparatus, we obtained the data of Fig. 4, which shows the metastable-atom current as a function of magnetic field. Superimposed on the signal, which is decreasing monotonically with field, are three distinct features which result from the anticrossing of magnetic substates of different lifetimes. The data were obtained by driving the x input of an x-y recorder with the rectified voltage generated by the rotating-coil magnetometer. The over-all quenching slope was reproducible to several percent, and the positions of the features to about 20 G, which was the precision of the magnetometer. The background signal present in all of these measurements (see FN for a discussion of this effect) was found to be independent of magnetic field and was neglected in subsequent analysis.

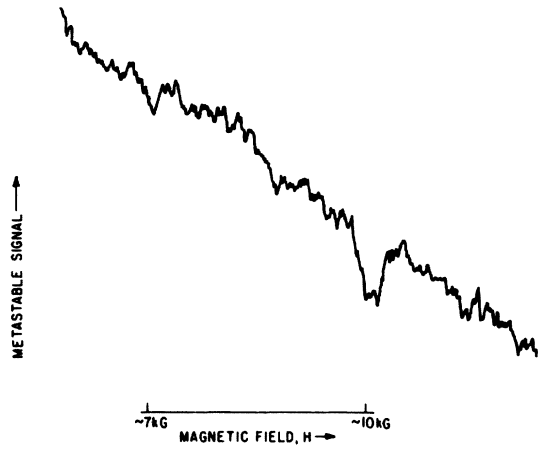

FIG. 4. Typical intermediate-field quenching curve for Li^7.

The three features observed on the Li^7 curve were studied in detail by using the CAT signal averager as described in the Sec. III. The results appear in Fig. 5. A careful investigation of Li^6 in the magnetic-field range 5–12 kG also yielded three features, as shown in Fig. 6. The anticrossing fields were obtained by assuming that the features are symmetric about the anticrossing point, an assumption which is perfectly valid for a two-level system.[10] Further justification was obtained from the detailed calculations described in Sec. V C. The asymmetric shapes of Figs. 5 and 6 result from the superposition of these features on a decreasing "continuum" signal. The total uncertainty in the values of the anticrossing fields due to noise, magnetic-field variations, and the systematic errors described in Sec. III is no greater than 2 G for the four narrow features on which the fine-structure analysis is based.

V. DISCUSSION OF RESULTS

A. $(1s2s2p)^4P$ Energy Matrix

In order to extract the physical quantities of interest from the data, we must suitably parametrize the matrix elements of the Hamiltonian. In Sec. V C, we will use this formalism to deal with the metastable decay rates. We first note that the matrix elements of interest are of the form $\langle\varphi_i|\mathcal{H}-\mathcal{H}'|\varphi_j\rangle$, where φ is a discrete-configuration eigenfunction of the Hamiltonian $\mathcal{H}'$ which contains only the kinetic energy and Coulomb-interaction terms, and $\mathcal{H}$ is the total Hamiltonian. It has been pointed out that despite the high energy of excitation ($E_\varphi = \langle\varphi|\mathcal{H}'|\varphi\rangle$) the states φ meet all the criteria for being classified as stationary.[15] It has been shown by Fano[16] that the mixing of the discrete configuration with a continuum configuration ψ_E (as described in Sec. II for our case) gives rise to a stationary state ψ whose energy is shifted from E_φ by an amount F, which is of the order of the energy width of ψ, as given by

$$\Delta E = 2\pi|V_E|^2 \equiv 2\pi|\langle\psi_E|\mathcal{H}|\varphi\rangle|^2 . \tag{3}$$

Since the auto-ionization lifetime τ is given by

$$\tau = \hbar/2\pi|V_E|^2 , \tag{4}$$

a level with a lifetime of 1 μsec will be shifted by about $F \approx \hbar/\tau \approx 5\times10^{-6}$ cm^{-1}. This shift is much smaller than the precision of the present work, and we are justified in using only the discrete components of the metastable eigenfunctions for determining the energy splittings.

We consider first the fine-structure operators. The spin-orbit (SO) and spin-other-orbit (SOO) terms are

$$\mathcal{H}_{so} = \sum_i \xi_i(r_i)\vec{l}_i\cdot\vec{s}_i , \tag{5}$$

where

$$\xi_i(r_i) = \frac{\hbar^2}{2m^2c^2}\frac{1}{r_i}\frac{\partial}{\partial r_i}\left(\frac{Ze^2}{r_i} - \sum_{j\neq i}\frac{e^2}{r_{ij}}\right); \tag{6}$$

and

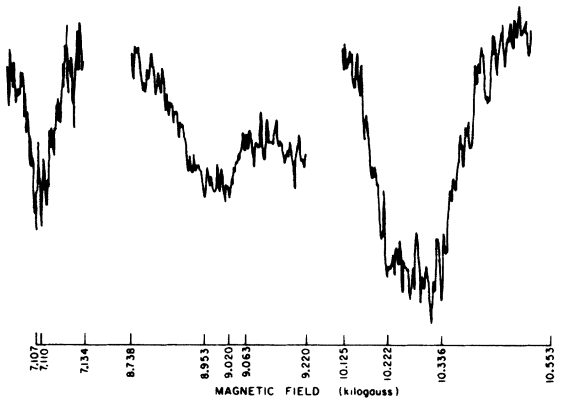

FIG. 5. Signal-averaged anticrossing data for Li^7.

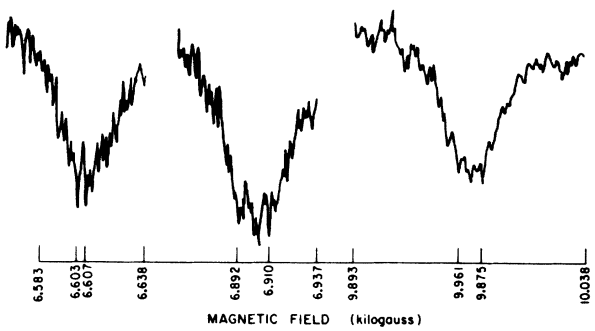

FIG. 6. Signal-averaged anticrossing data for Li^6.

$$\mathcal{H}_{soo} = \sum_{i \neq j} \eta(r_i) \vec{l}_i \cdot \vec{s}_j , \tag{7}$$

where

$$\eta = \frac{-\hbar^2}{m^2c^2} \frac{1}{r_i} \frac{\partial}{\partial r_i} \left(\frac{e^2}{r_{ij}} \right) . \tag{8}$$

The operators $\vec{l}_i$ and $\vec{s}_i$ are the orbital- and spin-angular-momentum operators for the ith electron, and r_{ij} is the interelectron distance. Since the energy difference between the quartet state and the nearest doublet is of the order of 1.3 eV [11] while $\mathcal{H}_{so}$ and $\mathcal{H}_{soo}$ are of the strength 10^{-4} eV, we can ignore the breakdown in LS coupling for the present in calculating the fine-structure splitting.

For the case of LS coupling, the matrix elements of the terms in $\mathcal{H}_{so}$ and $\mathcal{H}_{soo}$ are all proportional to the matrix elements of the operator $\vec{L} \cdot \vec{S}$, so that we have the relation

$$\mathcal{H}_{so} + \mathcal{H}_{SOO} = c_{so} \vec{L} \cdot \vec{S} . \tag{9}$$

If this were the only fine-structure operator, we would expect the fine-structure levels to be ordered according to the Landé-interval rule.

The orbit-orbit (OO) interaction is given by

$$\mathcal{H}_{OO} = \sum_{i > j} \tfrac{1}{2} \xi(r_i) \vec{l}_i \cdot \vec{l}_j . \tag{10}$$

This interaction is independent of J, and for the present case vanishes because only one electron has $l \neq 0$.

Finally, the spin-spin (SS) interaction between electrons is given by

$$\mathcal{H}_{ss} = 4 \mu_B \sum_{i > j} \left(\frac{\vec{s}_i \cdot \vec{s}_j}{r_{ij}^3} - \frac{3(\vec{r}_{ij} \cdot \vec{s}_i)(\vec{r}_{ij} \cdot \vec{s}_j)}{r_{ij}^5} - \frac{8\pi}{3} \vec{s}_i \cdot \vec{s}_j \delta(r_{ij}) \right) , \tag{11}$$

where

$$\mu_B = e\hbar / 2mc \quad \text{(Bohr magneton)} .$$

The contact part of the interaction shifts the ^4P energy, but does not affect the multiplet splitting, and can be ignored. If we put $\mathcal{H}_{SS}$ in tensor-operator form, [17] then within a given LS multiplet, $\mathcal{H}_{SS}$ has matrix elements given by

$$\mathcal{H}_{SS} = 3c_{SS} [(\vec{L} \cdot \vec{S})^2 + \tfrac{1}{2}(\vec{L} \cdot \vec{S}) - \tfrac{1}{3} S(S+1) L(L+1)] . \tag{12}$$

Hence $\mathcal{H}_{SS}$ is also diagonal in J. We can express the fs splittings

$$\Delta E_{53} = E_{J=5/2} - E_{J=3/2}$$

and

$$\Delta E_{51} = E_{J=5/2} - E_{J=1/2}$$

in terms of c_{SO} and c_{SS} as follows:

$$\Delta E_{53} = \tfrac{5}{2} c_{SO} + \tfrac{15}{2} c_{SS} , \tag{13a}$$

$$\Delta E_{51} = 4c_{SO} - 6c_{SS} . \tag{13b}$$

The interaction of the electrons with the nuclear magnetic moment (NMM) is

$$\mathcal{H}_{NMM} = 2\mu_B \mu_N g_N \sum_i \frac{1}{r_i^3} \vec{I} \cdot \left(\vec{l}_i - \vec{s}_i + \frac{3\vec{r}_i (\vec{r}_i \cdot \vec{s}_i)}{r_i^2} + \frac{8\pi}{3} \delta(\vec{r}_i) \vec{s}_i \right) , \tag{14}$$

where $\mu_N \approx \frac{1}{1836} \mu_B$ is the nuclear magneton; $\vec{I}$ is the nuclear-angular-momentum operator, and g_N is the nuclear moment in units of μ_N. The last term is the Fermi-contact term for s electrons, and the remainder of $\mathcal{H}_{NMM}$ gives the noncontact magnetic dipole (MD) interaction. Within an LS multiplet, one can reduce these operators to

$$\mathcal{H}_C = a_C \vec{I} \cdot \vec{S} \ \text{(contact)} , \tag{15}$$

$$\mathcal{H}_{MD} = a_{MD} \{ \vec{I} \cdot \vec{L} + [1/S(2L-1)(2L+3)] \times [L(L+1)(\vec{I} \cdot \vec{S}) - \tfrac{3}{2}(\vec{I} \cdot \vec{L})(\vec{L} \cdot \vec{S}) - \tfrac{3}{2}(\vec{L} \cdot \vec{S})(\vec{I} \cdot \vec{L})] \} . \tag{16}$$

It can also be shown that the diagonal matrix elements of the electric quadrupole interaction are

$$\mathcal{H}_Q = \frac{Qa_Q [3(\vec{I} \cdot \vec{J})^2 + \frac{3}{2}(\vec{I} \cdot \vec{J}) - I(I+1)J(J+1)]}{2I(2I-1)J(2J-1)} f_J , \tag{17}$$

where Q is the nuclear quadrupole moment and

$$f_J = -\langle J, M_J = J | 3\cos^2\theta - 1 | J, J \rangle ; \quad a_Q = \langle 1/r^3 \rangle ;$$

r and θ are coordinates of the $2p$ electron. [11] The expression for $\mathcal{H}_{MD}$ can only be written in the familiar form $\mathcal{H}_{MD} = A \vec{I} \cdot \vec{J}$ within a manifold of states of constant J. $\mathcal{H}_C$ and $\mathcal{H}_{MD}$ have diagonal matrix elements between states of the same F ($\vec{F} = \vec{I} + \vec{J}$) and J, and off-diagonal elements between states of the same F and different J. The angular matrix elements for these operators in the representation $[(SL)J, I, F, M]$ have been tabulated by Manson. [11]

When the atom is in an external magnetic field, the Zeeman operator must be included in the Hamiltonian. This is given by

$$\mathcal{H}_Z = (g_L L_Z + g_S S_Z - g_I' I_Z) \mu_B H , \tag{18}$$

where

$$g_I' = g_N \mu_N / \mu_B .$$

In the representation $[(SL)J, I, F, M]$, one finds that the Zeeman matrix elements are given by the expressions in Table I. Since the precision of the present experiment is not better than 1 part in 10^4, the parameters (ΔE_{53}, ΔE_{51}, a_C, a_{MD}, a_Q or c_{SO}, c_{SS}, a_C, a_{MD}, a_Q) are sufficient to specify the en-

TABLE I. Zeeman matrix elements in LS coupling.

$$\langle (SL)J, I, F, M \mid \mathcal{H}_Z \mid (SL)J, I, F, M\rangle = g_F \mu_B H M$$

$$g_F = g_J \frac{F(F+1)+J(J+1)-I(I+1)}{2F(F+1)} - g_I' \frac{F(F+1)+I(I+1)-J(J+1)}{2F(F+1)}$$

$$g_J = g_L \frac{L(L+1)+J(J+1)-S(S+1)}{2J(J+1)} + g_S \frac{S(S+1)+J(J+1)-L(L+1)}{2J(J+1)}$$

$$\langle (SL)J, I, F, M \mid \mathcal{H}_Z \mid (SL)J, I, F-1, M\rangle = \frac{(-)(g_J+g_I')\mu_B H}{2F}\left(\frac{(F^2-M^2)[(I+J+1)^2-F^2][F^2-(J-I)^2]}{(4F^2-1)}\right)^{1/2}$$

$$\langle (SL)J, I, F, M \mid \mathcal{H}_Z \mid (SL)J-1, I, F, M\rangle = \frac{(g_S-g_L)\mu_B H M}{4JF(F+1)}\left(\frac{[(I+F+1)^2-J^2][J^2-(F-I)^2][(L+S+1)^2-J^2][J^2-(L-S)^2]}{(4J^2-1)}\right)^{1/2}$$

$$\langle (SL)J, I, F, M \mid \mathcal{H}_Z \mid (SL)J-1, I, F-1, M\rangle = \frac{(g_S-g_L)\mu_B H}{4JF}\left(\frac{(F^2-M^2)[(J+F)^2-(I+1)^2][(J+F)^2-I^2][(L+S+1)^2-J^2][J^2-(L-S)^2]}{(4J^2-1)(4F^2-1)}\right)^{1/2}$$

$$\langle (SL)J, I, F-1, M \mid \mathcal{H}_Z \mid (SL)J-1, I, F, M\rangle = \frac{(-)(g_S-g_L)\mu_B H}{4JF}\left(\frac{(F^2-M^2)[(J-F)^2-(I+1)^2][(J-F)^2-I^2][(L+S+1)^2-J^2][J^2-(L-S)^2]}{(4J^2-1)(4F^2-1)}\right)^{1/2}$$

ergy matrix. Diagonalization of the matrix associated with each magnetic quantum number M for various magnetic fields H yields the dependence of the energy of the ith level on the field $[E_M(H)]_i$. The eigenfunctions corresponding to each level can also be obtained from the diagonalization process and can be expressed in the form

$$\psi_i^M(H) = \sum_{J,F} [a_{J,F}^M(H)]_i \mid (LS)J, I, F, M\rangle \ . \tag{19}$$

Manson[11] calculated the fine structure using antisymmetrized Hartree-Fock wave functions to obtain the results

$$\begin{aligned} E_{5/2} - E_{3/2} &= 0.575 \text{ cm}^{-1}, \\ E_{5/2} - E_{1/2} &= -2.610 \text{ cm}^{-1}, \\ c_{SO} &= -0.325 \text{ cm}^{-1}, \\ c_{SS} &= 0.185 \text{ cm}^{-1}. \end{aligned} \tag{20}$$

He also calculated numerical values for the hyperfine constants and obtained the results for Li^7:

$$\begin{aligned} a_C &= 0.172 \text{ cm}^{-1}, \\ a_{MD} &= 0.002\,05 \text{ cm}^{-1}, \\ c_Q &= Qa_Q = 1.05\times10^{-4} \text{ cm}^{-1}; \end{aligned} \tag{21}$$

and for Li^6:

$$\begin{aligned} a_C &= 0.065 \text{ cm}^{-1}, \\ a_{MD} &= 0.000\,78 \text{ cm}^{-1}, \\ c_Q &= 1.85\times10^{-6} \text{ cm}^{-1}. \end{aligned} \tag{22}$$

B. Determination of Fine- and Hyperfine-Structure Energy Constants

In order to determine the zero-field level scheme, it was assumed that the observed locations of the quenching structure correspond to the fields at which anticrossing-level pairs have minimum energy separation. According to von Neumann and Wigner,[10] the two anticrossing levels are most strongly coupled at this point, and the wave functions are equal combinations of the original wave functions. From our data, only four anticrossing fields could be determined accurately; therefore, to obtain a unique best fit to the data, only the three constants ΔE_{53}, ΔE_{51}, and a_C were considered free parameters while a_{MD} and a_Q were held fixed. The contact constants for the two isotopes scale by the ratio of nuclear g factors:

$$a_C(Li^6)/a_C(Li^7) = g_N(Li^6)/g_N(Li^7),$$

ignoring hfs-anomaly effects. For purposes of diagonalizing the energy matrix for various values of the variable energy parameters, we used the calculated values of a_{MD} and a_Q and the values

$$\begin{aligned} g_S &= 2.002\,32, \quad g_L = 1.000\,0(1 - m_e/M_{Li}), \\ g_N(Li^7) &= 2.170\,65, \\ g_N(Li^6) &= 0.821\,92, \text{ (Ref. 18)} \\ \mu_B &= 0.046\,685\,97 \text{ cm}^{-1}/\text{kG}. \end{aligned} \tag{23}$$

Then the $\frac{5}{2}-\frac{1}{2}$ and $\frac{5}{2}-\frac{3}{2}$ zero-field fine-structure splittings and a_C were varied to minimize the quantity

$$\mathcal{S}^2 = \sum_{i=1}^{4} (H_i^c - H_i^e)^2, \tag{24}$$

where H_i^c and H_i^e are, respectively, the calculated and experimental values of the ith anticrossing field. In practice, the calculated anticrossing fields H_i^c were expressed in terms of the energy parameters which we here denote by x_j:

$$H_i^c = H_i^c(x_j^0) + \sum_{j=1}^{3} \left(\frac{\partial H_i}{\partial x_j}\right)_{x_j^0} \delta x_j \,. \tag{25}$$

The derivatives were determined by diagonalizing the energy matrix, using a set of values x_j^0; the variations in the x_j were found which gave the best fit to the data. This process was repeated using the calculated $x_j^0 + \delta x_j$ and converged rapidly to a final set of values. Similarly, the uncertainties in the x_j were determined in terms of the probable errors in the experimental values of the anticrossing fields.

It was also necessary to estimate the error which is introduced if the actual value of a_{MD} is substantially different from the calculated value. The value of a_{MD} depends on the quantity $\langle r_{2p}^{-3} \rangle$, which has been calculated by Goodings[19] for the $(1s^2 2p)\ ^2P_{1/2}$ state of Li^7, using Hartree theory. Goodings's value is found to be in good agreement with the value determined from the level-crossing experiment of Brog, Eck, and Wieder,[20] so that at least in the one-electron case the Hartree theory seems to be valid.

For the extreme case of $a_{MD} = 0$, a best fit to the anticrossing data was obtained with shifts of

$$\begin{aligned} |\delta(E_{5/2} - E_{1/2})| &= 0.086 \text{ mK}, \\ |\delta(E_{5/2} - E_{3/2})| &= 0.058 \text{ mK}, \\ |\delta a_C(Li^7)| &= 0.33 \text{ mK}, \end{aligned} \tag{26}$$

from the values obtained using the calculated value of a_{MD}. We have introduced the unit of the milli-Kaiser (1 mK = 10^{-3} cm^{-1}) here for convenience. Since these energy shifts are only a fraction of the experimental uncertainties in the energy parameters, any reasonable uncertainty in the magnetic dipole term may be safely disregarded.

The energies of the $J = \frac{3}{2}$ and $J = \frac{1}{2}$ fs levels are also shifted by their mixing with the doublets. The energy shift due to mixing with the nearest doublet, denoted by $^2P_J^-$, is given by perturbation theory as

$$\Delta W_J = |\langle {}^4P_J | \mathcal{H}_{fs} | {}^2P_J^- \rangle|^2 / [E(^2P^-) - E(^4P)] \,. \tag{27}$$

We estimate these to be $\Delta W_{3/2} = 0.2$ mK and $\Delta W_{1/2} = 0.6$ mK. These quantities are used to correct for the values of c_{SS} and c_{so} obtained from the best-fit fine-structure splittings by using Eqs. (13a) and (13b). The uncertainties in the values of ΔW_J, taken to be $\pm \Delta W_J$, must be combined with the errors in ΔE_{53} and ΔE_{51} to determine the total errors in c_{SO} and c_{SS}.

To the present experimental accuracy, we are justified in assuming that the fine-structure splittings in Li^6 and Li^7 are equal. The electron-nucleus spin-orbit contribution to the splittings is actually contracted by the ratio of the reduced mass to the electronic mass, so that this contribution to the fine-structure splittings for the isotopes is in the same ratio as their reduced masses. Since this gives a difference of about 1 part in 10^5, it can be ignored.

The results for the experimental anticrossing fields, the calculated fields giving the best fit, the level identifications, and the calculated energy parameters, as well as theoretical values for comparison, are given in Tables II and III. The behavior of the energies and amplitudes of the observed anticrossing levels in Li^7 is shown in Fig. 7. As noted above, the energy intervals have been verified by the identification[5] of two multiplets in the spectrum[6] of Li which result from the transitions $(1s\,2s\,3s)\ ^4S - (1s\,2s\,2p)\ ^4P$ and $(1s\,2p^2)\ ^4P^e - (1s\,2s\,2p)\ ^4P$.

It can be seen from Tables II and III that the only serious disagreement between experiment and Manson's calculation is in the value of c_{so}. The fact that the sign is negative indicates that the spin-orbit and spin-other-orbit terms arising from relative motion of pairs of electrons dominate the electron-nucleus terms. This is consistent with the theoretical and experimental results for the $(1s\,2p)\ ^3P$ levels in He and Li^+. The calculations[21] for He indicate that the effect of the inner electron overcompensates that of the nucleus, so that the spin-orbit constant is negative. The observed ordering[21] of the fine-structure levels ($J = 0, 1, 2$) is therefore totally inverted, with the $J = 1$ and $J = 2$ levels being almost degenerate because of the smaller spin-spin interaction. For Li^+, the experimental results[6] indicate that the spin-orbit constant is only $+0.009$ cm^{-1}, and the ordering of the levels which is determined by the spin-spin interaction is partially inverted. The theory of Bethe and Salpeter[22] predicts no spin-orbit splitting for Li^+. The present results indicate that the addition of the $2s$ electron swings the balance back in favor of the interelectron spin-orbit terms for the ^4P level. Since, however, c_{SS} is larger in magnitude than c_{so}, the level ordering is the same as for Li^+. The experimentally determined splittings for the three cases (He, Li^+, Li) appear in Fig. 8.

TABLE II. Experimental and calculated anticrossings for ^4P state of lithium.

Isotope	H_c(kG) (experiment)	H_c(kG) (calculated)	Zero-field quantum numbers of anticrossing levels		
			J, F	J', F'	$M_F = M_{F'}$
Li^7	7.111 ± 0.002	7.110	$\frac{5}{2}, 4$	$\frac{1}{2}, 1$	1
	8.978 ± 0.010	8.977	$\frac{5}{2}, 3$	$\frac{1}{2}, 1$	1
	10.280 ± 0.005	10.280	$\frac{5}{2}, 4$	$\frac{1}{2}, 1$	0
Li^6	6.607 ± 0.002	6.607	$\frac{5}{2}, \frac{3}{2}$	$\frac{3}{2}, \frac{5}{2}$	$-\frac{1}{2}$
	6.901 ± 0.002	6.900	$\frac{5}{2}, \frac{3}{2}$	$\frac{3}{2}, \frac{5}{2}$	$\frac{1}{2}$
	9.968 ± 0.002	9.969	$\frac{5}{2}, \frac{7}{2}$	$\frac{1}{2}, \frac{1}{2}$	$\frac{1}{2}$

TABLE III. Fine-structure splitting and fine and hyperfine constants for ^4P state of lithium (in mK).

Quantity	Experiment (this work)	Theory [a]
$E_{5/2}-E_{1/2}$	-1724.70 ± 0.54	-2610
$E_{5/2}-E_{3/2}$	$+997.34\pm0.66$	$+575$
c_{SO}	-154.47 ± 0.30	-325
c_{SS}	$+184.47\pm0.14$	$+185$
$a_C(Li^7)$	$+172.09\pm1.12$	$+172$
$a_C(Li^6)$	65.16 ± 0.42	$+65$

[a] See Manson, Ref. 11.

C. $J=\frac{3}{2}$ and $J=\frac{1}{2}$ Lifetimes

In this section, we will use the wave functions of the form (19) to determine the lifetimes from the observed widths of the anticrossing curves. First, we must justify using a time-independent theory in which we ignore the natural widths due to the decay of the interacting levels. Bethe and Salpeter[23] have shown that one can ignore the level widths in calculating the decay rates of two coupled states, separated by energy $\hbar\omega$, if the condition $4\omega\tau_s \gg 1$ is satisfied, where τ_s is the lifetime of the shorter-lived of the two states. The smallest value of $\hbar\omega$ is ≈ 0.3 mK so that we require $\tau_J \gg 4.3\times10^{-9}$ sec. We will see later in the section that this is so, and therefore, that the time-independent theory is applicable.

The decay rate $\gamma_i(H)$ of the ith metastable state of Li^7 is given by a weighted sum of the decay rates γ_J of the pure fs levels ^4P_J:

$$\gamma_i(H)=\gamma_{5/2}\sum_{F=1}^{4}[a^M_{5/2,F}(H)]_i^2+\gamma_{3/2}\sum_{F=0}^{3}[a^M_{3/2,F}(H)]_i^2+\gamma_{1/2}\sum_{F=1}^{2}[a^M_{1/2,F}(H)]_i^2\ , \tag{28}$$

where the expansion coefficients $[a^M_{J,F}(H)]_i$ are obtained by diagonalization of the Li^7 energy matrix using the fine and hyperfine energy constants obtained in Sec. V B. There is no interference between the various J decay channels so long as the hyperfine interaction which couples quartet and doublet states is negligible, and cross terms of the form $[\pm(a^M_{J,F})_i(a^M_{J\pm1,F})_i(\gamma_J\gamma_{J\pm1})^{1/2}]$ can be ignored. The calculations of Manson[11] indicate that this is the case.

The number of metastable atoms in state i reaching a distance x from the excitation source is given in terms of the number at the source, $N(0)$, by

$$N(x)/N(0)=\int_0^\infty f(u)e^{-a_i/u}\,du\ . \tag{29}$$

Here $u=v/\alpha$, $\alpha=(2kT/m)^{1/2}$ is the most probable velocity in the beam, and $a_i=x\gamma_i(H)/\alpha$. The normalized velocity distribution $f(u)$ was assumed to be Maxwellian. However, Pearl, Donnelly, and Zorn[24] have recently shown that a proper account of electron recoil and excitation geometry leads to a narrow double-peaked velocity distribution of metastable atoms produced by electron impact. In the case of our experimental geometry, the poor collimation of the ground-state lithium beam, the relatively large solid angle of the detector, and the energy spread of the incident electron beam all tend to smear out the velocity distribution and restore the Maxwellian form of the ground-state beam distribution. In lieu of a direct measurement of the velocity distribution made at the time of the anticrossing measurements, we have used the formulation of Pearl *et al.*,[24] assuming only s-wave scattering, to estimate the uncertainty in our results obtained by assuming a Maxwellian velocity distribution in fitting the data. Only the lifetimes are affected and by no more than 20%. The results of Sec. V E and VI are unaffected by the choice of velocity distribution provided that the same distribution is used consistently in all of the calculations.

In order to determine the lifetimes of the $J=\frac{3}{2}$ and $J=\frac{1}{2}$ fs levels, expressions (28) and (29) were used for a pair of anticrossing levels, and the appropriate parameter ($\gamma_{3/2}$ or $\gamma_{1/2}$) was varied to compute a theoretical anticrossing line shape which best fits the data. It was assumed that the anticrossing levels have equal excitation cross sections, and the corrected experimental value for $\gamma_{5/2}$ discussed in Sec. V D was used. It was found that the theoretical half-width, i.e., full width at half-maximum, of a given anticrossing signal varied monotonically with the value of γ_J. Theoretical curves for several anticrossings appear in Figs. 9(a) and 9(b), where the variation of width with γ_J can be seen. In the figure, β_J is the dimensionless ratio $\gamma_J/\gamma_{5/2}$. A comparison of the theoretical and experimental line shapes is shown in Fig. 9(c). The experimental half-widths and the values of the γ_J's giving the best fit of theory to experiment are given in Table IV.

The values for $\gamma_{3/2}$ from the two lowest crossings in Li^6 are in very good agreement. However, the two values for $\gamma_{1/2}$ do not seem to be consistent. A possible cause of this discrepancy is the mass dependence on the velocity distribution of the metastable atoms. This was investigated using the formalism of Pearl *et al.*[24] to calculate the velocity distribution for the two lithium isotopes for the geometry of our experiment, and was found to have little effect on the relative values of $\gamma_{1/2}$ obtained from the Li^7 and Li^6 data. Even the assumption of perfect collimation was insufficient to reconcile the two values of $\gamma_{1/2}$. Furthermore, data taken by moving the detector parallel to the metastable beam give a value of $\gamma_{5/2}$ which agrees with the value of FN to within the observational error. Since the two determinations of $\gamma_{5/2}$ were made with quite

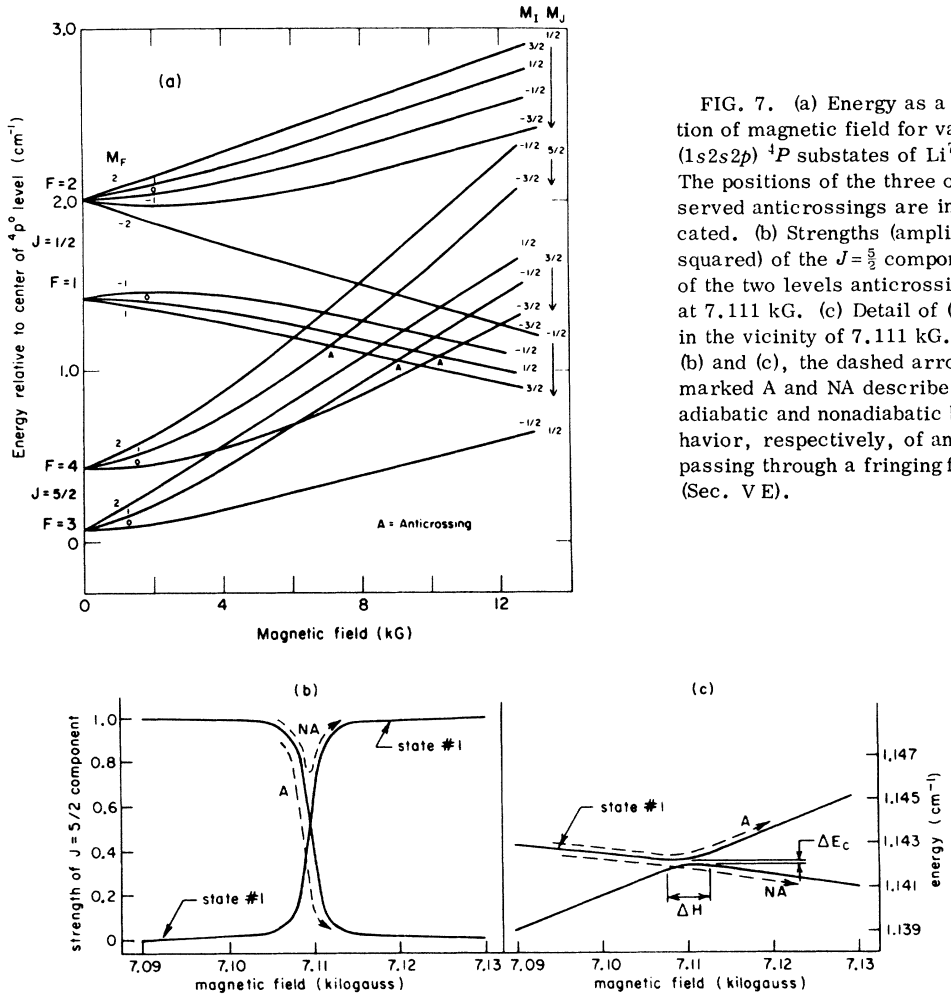

FIG. 7. (a) Energy as a function of magnetic field for various $(1s2s2p)\ ^4P$ substates of Li^7. The positions of the three observed anticrossings are indicated. (b) Strengths (amplitudes squared) of the $J=\frac{5}{2}$ components of the two levels anticrossing at 7.111 kG. (c) Detail of (a) in the vicinity of 7.111 kG. In (b) and (c), the dashed arrows marked A and NA describe the adiabatic and nonadiabatic behavior, respectively, of an atom passing through a fringing field (Sec. V E).

different excitation geometries, the effect of recoil on the velocity distribution must have been less than the observational error. Even so, in the absence of direct measurements of the velocity distribution, it is not possible to exclude this possible cause of the discrepancy.

Other possible sources of error, such as the uncertainty in the magnetic dipole term or a nonuniform population of the magnetic substates due to "bombardment polarization" (see Sec. V E) were found to be incapable of resolving the discrepancy. One other possibility, which is difficult to evaluate quantitatively, [11] is that Eq. (28) is not valid for the $\frac{5}{2}-\frac{1}{2}$ anticrossings in Li^7 due to an anomalously large quartet-doublet hyperfine coupling. Since the inconsistency in $\gamma_{1/2}$ cannot at present be resolved, a relatively large uncertainty is assigned to its value. The experimentally derived values for the lifetimes are given in Table V along with theoretical results. It can be seen that there is reasonably good agreement between theory and experiment for $\tau_{5/2}$ and $\tau_{3/2}$, but the value of $\tau_{1/2}$ which we have measured is considerably smaller than the theoretically predicted values.

In Fig. 10, we plot the Z dependence of various theoretical and experimental values τ_J for the $(1s\,2s\,2p)$ isoelectronic series. If the theory of Balashov *et al.* [12] is plotted in the form $\gamma_J{}^{1/n}$ versus Z, where n is a whole number and Z is the atomic number, it is found that a best fit to linear dependence is obtained for $J=\frac{5}{2}$ when $n=3$ and for $J=\frac{3}{2}$, $\frac{1}{2}$ when $n=6$. This is analogous to the Z dependence of the spin-spin and spin-orbit interaction energies, respectively, for the case of hydrogenic electron orbitals. The plots appear in Figs. 10(a) and 10(b). The experimental results for $J=\frac{5}{2}$ states with Z ranging 2–8 seem to obey the same power dependence as the theory, but with different slope and intercept. The experimental results can be approximately represented by the empirically derived expression

$$\gamma(^4P_{5/2}) = (1.13\times10^5)(Z-1.75)^3\ \text{sec}^{-1}. \qquad (30)$$

The experimental results for $J<\frac{5}{2}$ do not extend

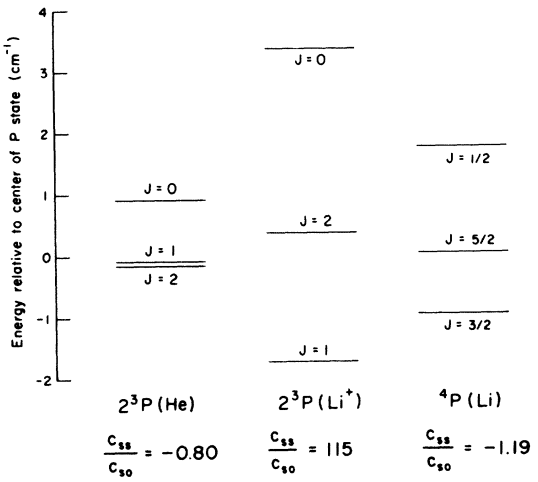

FIG. 8. Fine-structure splitting of 2^3P states in He and Li^+ and of the ^4P state in Li.

to high enough Z values to justify any definitive statement about the Z dependence of γ. However, it can be seen from Fig. 10(b) that the results indicate the shorter-lived component of Be^+ observed by Dmitriev *et al.*[25] to be associated with a $J=\frac{3}{2}$ level. Moreover, the three available $J=\frac{3}{2}$ points are quite colinear when plotted in the form $\gamma^{1/6}$ versus Z. If the available data are assumed to satisfy the same power law given by theory, the following crude approximations are obtained:

$$\gamma(^4P_{3/2}) \cong (6.75\times10^3)(Z-0.4)^6 \text{ sec}^{-1},$$
$$\gamma(^4P_{1/2}) \cong (1.1\times10^5)(Z-1.0)^6 \text{ sec}^{-1}. \quad (31)$$

D. $J=\frac{5}{2}$ Lifetime

In FN, the lifetime of the $(1s2s2p)\,^4P_{5/2}$ state was determined by a time-of-flight method under the assumption that the beam consisted only of atoms in the long-lived $J=\frac{5}{2}$ state. However, for Li^7, even at zero magnetic field there is significant hyperfine mixing of the fine-structure states, so that the measured beam contains atoms with lifetimes somewhat shorter than the $J=\frac{5}{2}$ value. Hence, the value of τ derived from the data in FN is actually less than the correct value. Figure 11 shows the calculated beam intensity as a function of distance from the source (in units of a decay length $a=x\gamma_{5/2}/\alpha$) for Li^7, Li^6, and the hypothetical case of no hyperfine structure (corresponding to the computation of FN). It is clear that the lifetime of FN, which was based on Li^7 data, is too small and that the excitation cross section derived from these data is also too small by a factor of 2.

In order to take into account the zero-field mixing, it is necessary to know the ratios of the $J=\frac{3}{2}$ and $\frac{1}{2}$ lifetimes to the $J=\frac{5}{2}$ lifetime, but these quantities, as evaluated in Sec. V C, depend on the actual value of $\tau_{5/2}$. An iterative procedure must be used to determine a self-consistent set of values for the lifetimes. Fortunately, this procedure con-

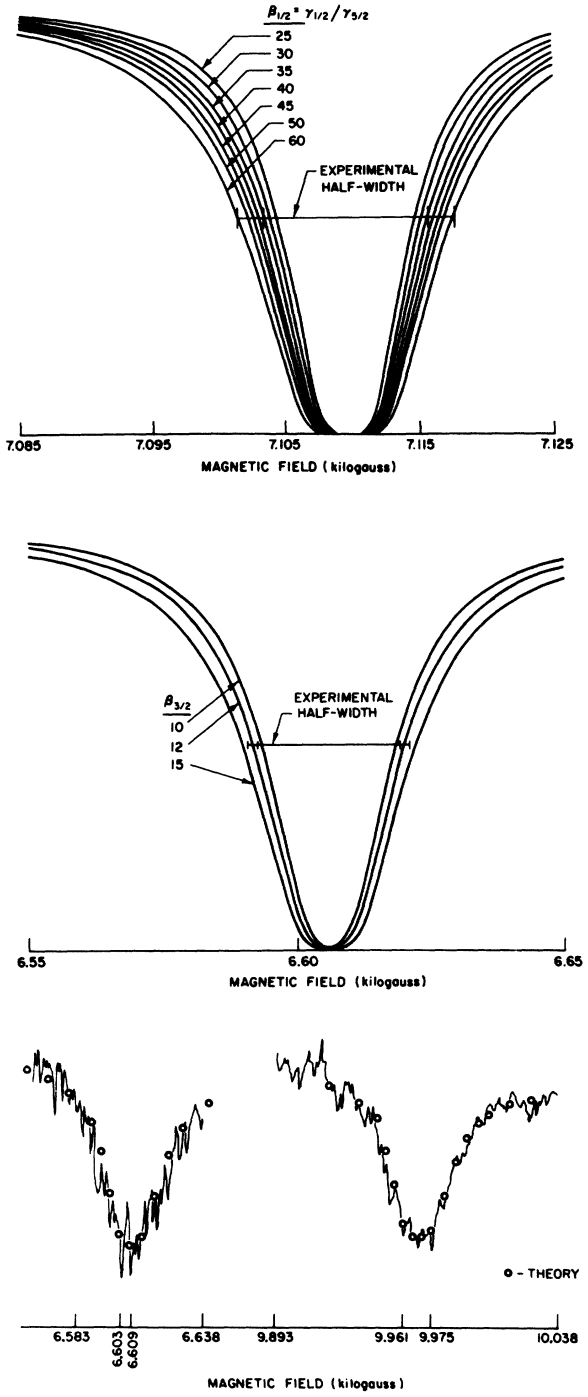

FIG. 9. (a) Calculated line shape of the 7.111-kG anticrossing in Li^7 for various values of $\beta_{1/2}\equiv\gamma_{1/2}/\gamma_{5/2}$. (b) Calculated line shape of the 6.607-kG anticrossing in Li^6 for various values of $\beta_{3/2}\equiv\gamma_{3/2}/\gamma_{5/2}$. (c) Comparison of calculated line shapes with experimental results.

TABLE IV. Decay rates derived from anticrossing widths.

Isotope	H_c	Experimental width (G)	J	γ_J ($\times 10^6$ sec^{-1})
Li^6	6.607	28.6±2.0	$\frac{3}{2}$	2.18±0.25
Li^6	6.901	37.1±2.0	$\frac{3}{2}$	2.18±0.25
Li^6	9.968	34.3±2.0	$\frac{1}{2}$	5.18±0.78
Li^7	7.111	14.4±2.0	$\frac{1}{2}$	8.35±2.45

verges very rapidly with changes of less than 1% in the lifetimes after two iterations. The results have already been summarized in Sec. V C. It should be noted that the major uncertainty in $\tau_{5/2}$ arises from the uncertainty in the velocity distribution of the beam of metastable atoms.

E. Quenching in a Nonuniform F_z

Finally, we wish to reconsider the data of Fig. 2 In this experiment, the metastable beam was produced in a field of 1 kG. The beam traveled in a field-free region a distance of about 1 cm beyond the edge of the magnet producing this field and then passed through a plane defining the edge of the quenching magnet. The pole tips of the quenching magnet were spaced 0.5 mm apart. For this geometry, empirical data on fringing fields[26] indicate that the field gradient at the edge of the quenching magnet is about $5H$ (G/cm), where H is the value of the quenching field in gauss. For an atom with a velocity of 1.35×10^5 cm/sec, the variation of field with time dH/dt is equal to $6.5\times10^5 H$ (G/sec).

Imagine now that H is set at some value a little higher than one of the anticrossing fields H_c. Since there is a strong field gradient, we must consider the possibility that an atom in one of the anticrossing levels undergoes a Majorana transition to the other level as it passes through H_c. Most of the atoms entering the quenching magnet will be in the state that is long-lived at low field. If a nonadiabatic transition occurs in the fringing field of the magnet, the atoms will still be in the longer-lived of the two states in the quenching region, and the signal will increase at fields above that particular H_c. Otherwise, the atom will follow the continuous energy versus field trajectory and will find itself in the shorter-lived state for fields above H_c. This behavior is illustrated by the dashed arrows labeled

TABLE V. Experimental and theoretical ^4P_J lifetimes ($\times10^{-6}$ sec) for Li.

Lifetime	Experiment		Theory	
$\tau_{5/2}$	5.8±1.2	5.88[a]	7.20[b]	7.60[c]
$\tau_{3/2}$	0.46±0.10	0.30[a]	0.85[b]	
$\tau_{1/2}$	0.14±0.07	>10.0[a]	2.40[b]	

[a] See Manson, Ref. 11.

[b] See Balashov *et al.*, Ref. 12.

[c] C. Laughlin and A. L. Stewart, J. Phys. B 1, 151 (1968).

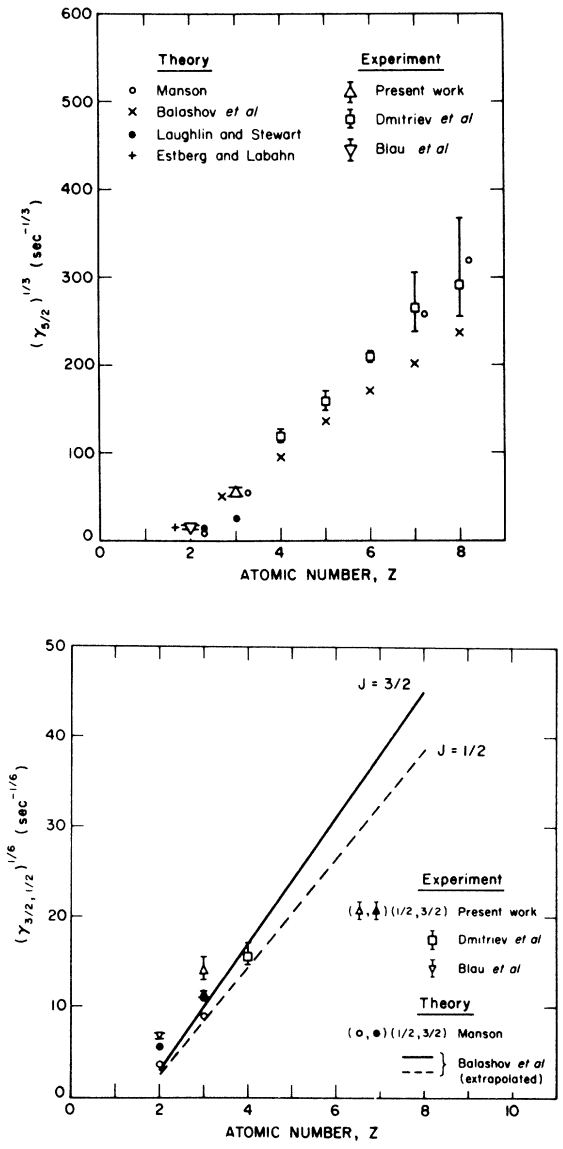

FIG. 10. (a) Theoretical and experimental decay rates for the $J=\frac{5}{2}$ states of the $(1s2s2p)\,^4P$ isoelectronic series Experimental: Δ, present work; □, Ref. 25; ∇, Ref. 32. Theoretical: o, Ref. 9; ×, Ref. 12; ●, see footnote c of Table V; +, G. N. Estberg and R. W. LaBahn, Phys. Letters 28A, 420 (1968). (b) Decay rates for the $J=\frac{3}{2}$ and $J=\frac{1}{2}$ states. Experimental: (Δ, ▲), present work ($J=\frac{1}{2}$, $J=\frac{3}{2}$); □, Ref. 25 (J not specified); ∇, Ref. 32(weighted average of $J=\frac{1}{2}$ and $J=\frac{3}{2}$). Theoretical: (o, ●), Ref. 11 ($J=\frac{1}{2}$, $J=\frac{3}{2}$); (---, ——), Ref. 12 ($J=\frac{1}{2}$, $J=\frac{3}{2}$).

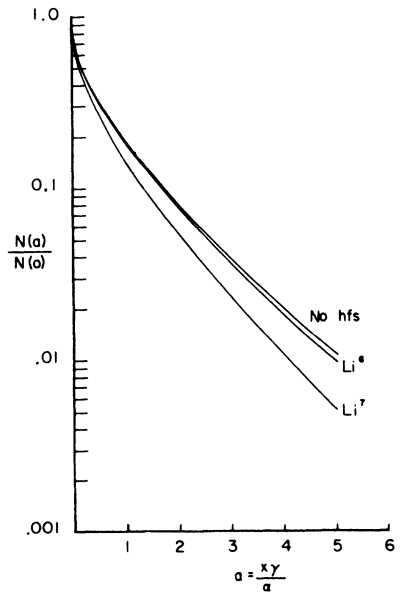

FIG. 11. Relative metastable signal versus number of decay lengths showing effect of hfs.

NA (nonadiabatic) and A (adiabatic) in Figs. 7(b) and 7(c). We thus expect a nearly symmetric dip if a transition occurs, and a sharp falloff with no recovery if no transition occurs. There will be no transition if the adiabatic criterion is satisfied, i.e., if the atom stays in a region ΔH a time long compared with the time $h/\Delta E_c$. Here ΔE_c is the minimum energy separation between levels at the anticrossing point; ΔH is the "width" of the anticrossing[10] and is the difference in field values for which the energy separation is $\Delta E = 2\Delta E_c$. Thus, for no transition, we require

$$\Delta t = \Delta H \Big/ \frac{dH}{dt} \gg \frac{h}{\Delta E_c}, \tag{32a}$$

or

$$k_A \equiv \frac{h}{\Delta H}\frac{dH}{dt}\frac{1}{\Delta E_c} \gg 1, \tag{32b}$$

where k_A is defined as the "adiabatic parameter." Table VI lists all of the anticrossings up to 20 kG for both Li^6 and Li^7 and gives the values of ΔE_c, ΔH, and k_A for each. Those anticrossings which do not satisfy the adiabatic criterion are denoted by an asterisk.

The calculations of Sec. V C can be extended to include a summation over all substates in order to calculate the fraction of the metastable beam reaching a given distance. If D is the field-free drift distance and L the effective length of the magnet, the dimensionless decay constant appearing in Eq. (29) must be replaced by

$$a = [\gamma_i(H=0)D + \gamma_i(H)L]/\alpha .$$

In evaluating the $\gamma_i(H)$, care must be taken to switch

TABLE VI. Calculated anticrossings and adiabatic parameters.

Isotope	H_c(kG)	M_F	ΔH(G)	ΔE_c(mK)	k_A	Expected Transitions
Li^7	1.860	−1	19.2	0.859	2.54	*
	3.098	0	81.3	3.13	0.27	
	4.461	−1	76.2	3.13	0.42	
	4.713	−2	133	4.60	0.17	
	5.485	0	134	5.19	0.18	
	5.804	1	406	12.6	0.03	
	5.988	−1	393	12.9	0.03	
	7.110	1	4.96	0.282	115.	*
	7.634	0	634	22.0	0.01	
	8.977	1	75.1	3.56	0.76	
	10.280	0	102	4.38	0.52	
	17.887	2	293	8.94	0.15	
	18.846	1	334	10.5	0.12	
Li^6	6.108	$-\frac{3}{2}$	8.71	0.334	47.2	*
	6.607	$-\frac{1}{2}$	22.3	0.839	7.96	*
	6.900	$\frac{1}{2}$	30.4	1.22	4.18	*
	9.969	$\frac{1}{2}$	15.5	0.763	19.0	*
	15.985	$\frac{3}{2}$	31.9	1.03	11.0	*
	16.395	$\frac{1}{2}$	287	10.4	0.12	
	16.777	$\frac{1}{2}$	806	22.7	0.02	
	17.401	$-\frac{1}{2}$	865	23.9	0.02	

pairs of eigenfunctions for those states that interchange (*) at the anticrossings, for all fields greater than the anticrossing field.

The results of these calculations are shown in Fig. 12 for Li^7 and Fig. 13 for Li^6. Two solid curves are shown in each case, using the value of 4 cm for D. The upper curve is calculated for a uniform population of magnetic substates. In the lower curve, each substate is weighted by its fractional composition of $M_L = 0$. This corresponds to the "bombardment-polarization" effect for electron-impact excitation at threshold.[27] The experimental data of Fig. 2 are replotted on Figs. 12 and 13. The Li^7 data, for the most part, fall be-

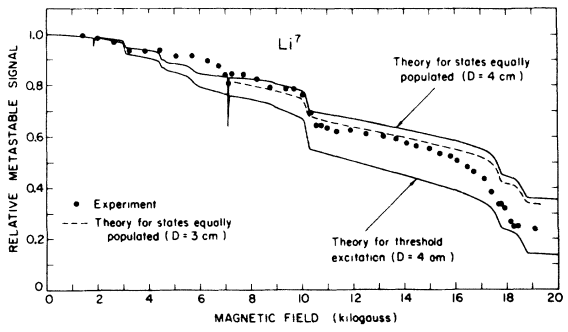

FIG. 12. Theoretical and experimental Zeeman-quenching curves for Li^7. The data in Figs. 12 and 13 are the same as in Fig. 2.

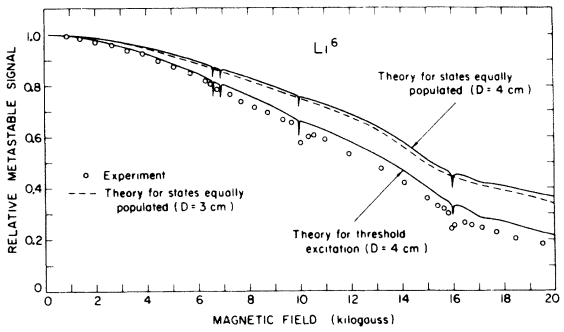

FIG. 13. Theoretical and experimental Zeeman-quenching curves for Li^6. Structure is suppressed on the dashed curve.

tween the two calculated curves, with practically all of the features of the data reproduced by the theoretical curves. A curve calculated for equal state populations and $D = 3$ cm is also shown in the figures. Bombardment polarization is clearly important since the cross section for excitation to the ^4P states is peaked very sharply only 0.9 eV above threshold.[1] A calculation of bombardment polarization at any energy above threshold, however, is beyond the scope of the present work. The importance of this effect can be seen even more strikingly in Fig. 13 for Li^6. There is very good agreement between the data and the theoretical curve incorporating threshold excitation cross sections. It is clear that any error in D is unimportant. Despite the poor magnetic-field resolution due to the fringing fields of the quenching magnet, most of the predicted quenching features are observed.

VI. PRODUCTION OF POLARIZED LITHIUM NUCLEI

It was suggested earlier[28] that the differential metastability of the $(1s\,2s\,2p)\,^4P$ levels would provide a possible mechanism for producing polarized electrons and nuclei, especially those of He^3 ($I = \frac{1}{2}$) and Li^6 ($I = 1$). If in a strong magnetic field a beam of metastable atoms traversed a sufficient number of decay lengths, only those atoms in states of magnetic quantum number $M_F = \pm\frac{7}{2}$ (for Li^6) would not be significantly quenched by mixing with the shorter-lived states. These levels are associated with the nuclear orientations given by $M_I = \pm 1$, respectively, and could be separated from each other in an inhomogeneous magnetic field. It was assumed that the $J = \frac{5}{2}$ levels having $M \neq \frac{7}{2}$ would become increasingly mixed with $J = \frac{3}{2}$ components at higher fields. However, this mixing process is not monotonic with increasing magnetic field. At fields high enough for the angular momenta L, S, and I to become uncoupled, there is a long-lived state corresponding to each possible nuclear-spin orientation. The question then is whether some range of intermediate fields exists at which the mixing of the zero-field eigenfunctions can cause significant nuclear polarization without requiring the beam to travel a prohibitive number of decay lengths. We can treat this problem analytically by using the results of Sec. V.

For a particle with spin 1, such as a Li^6 nucleus, the spin operator $\underline{S}$ is represented by the matrices

$$S_1 = \frac{\hbar}{\sqrt{2}}\begin{pmatrix} 0 & 1 & 0 \\ 1 & 0 & 1 \\ 0 & 1 & 0 \end{pmatrix}, \quad S_2 = \frac{\hbar}{\sqrt{2}}\begin{pmatrix} 0 & -i & 0 \\ i & 0 & -i \\ 0 & i & 0 \end{pmatrix},$$

$$S_3 = \hbar\begin{pmatrix} 1 & 0 & 0 \\ 0 & 0 & 0 \\ 0 & 0 & -1 \end{pmatrix}. \tag{33}$$

When the axes of reference are rotated, the 3×3 density matrix describing a beam of spin-1 particles has some components which transform like a vector and others which transform like a tensor. The vector polarization is defined by

$$P = (1/\hbar)\,\langle \underline{S} \rangle\ , \tag{34}$$

and the tensor polarization, by

$$P_{ij} = (3/2\hbar^2)(\langle S_i S_j \rangle + \langle S_j S_i \rangle) - 2\delta_{ij}. \tag{35}$$

When the three axes of a Cartesian system are chosen to satisfy the condition

$$\tfrac{1}{2}\langle S_1^2 \rangle x_1^2 + \tfrac{1}{2}\langle S_2^2 \rangle x_2^2 + \langle S_3^2 \rangle x_3^2 = 1, \tag{36}$$

the vector and tensor polarizations are

$$\begin{aligned} &P_1 = P_2 = 0, \\ &P_3 = N_{+1} - N_{-1}, \\ &P_{12} = P_{23} = P_{31} = 0, \\ &P_{11} = P_{22} = \tfrac{1}{2}(3N_0 - 1), \\ &P_{33} = 3(N_{+1} + N_{-1}) - 2 = -2P_{11}, \end{aligned} \tag{37}$$

where N_{+1}, N_0, and N_{-1} are the occupation numbers of nuclei in the beam corresponding to $M_I = +1$, 0, -1, respectively, and satisfy

$$N_{+1} + N_0 + N_{-1} = 1. \tag{38}$$

Consider an ensemble of nuclei whose spins are coupled to the electronic angular momenta in a beam of metastable atoms which are traveling in a region in which there is a uniform magnetic field $H\hat{x}_3$. Then the occupation number N_i is defined by

$$N_i(x,H) = \sum_j Q_j f_j(x,H) \sum_{J,F} \left| [a_{J,F}(H)]_j\, C^{J,I,F,M_F}_{J,(M_F - M_I^i),I,M_I^i} \right|^2$$

$$\times \sum_{i'} \left(\sum_j Q_j f_j(x,H) \sum_{J,F} \left| [a_{J,F}(H)]_j\, C^{J,IF,M_F}_{J,(M_F - M_I^{i'}),I,M_I^{i'}} \right|^2 \right). \tag{39}$$

The index j ranges over all the metastable states with eigenfunctions

$$\psi_j = \sum_{J,F} [a_{J,F}(H)]_j \mid J, I, F, M_F \rangle .$$

Q_j is the cross section for excitation of the jth state, and f_j is the fraction of atoms in the jth state which have not decayed at a distance x from the point of production. If we assume that the metastables are excited at essentially one point in space, then for an atom with velocity v, we have

$$f_j(x, H) = e^{-x/j(H)x/v} . \tag{40}$$

The Clebsch-Gordan coefficients of interest are given by

$$C^{J,I,F,M_F}_{J,M_J,I,M_I} = (-)^{J-I+M_F}(2F+1)^{1/2}\begin{pmatrix} J & I & F \\ M_J & M_I & -M_F \end{pmatrix} \tag{41}$$

and are tabulated in Table VII.

If we assume that the excitation process populates all states equally, we can calculate the polarization in the beam as a function of x and H using the previously determined wave functions and lifetimes. The results obtained by integrating over the velocity distribution appear in Fig. 14 for various values of $\alpha = x\gamma_{5/2}/\alpha$. It can be seen that the tensor polarization P_{33} has a broad maximum at about 16 kG, and that the vector polarization P_3 has a narrow maximum at this field. Both features are clearly related to the anticrossings discussed in Sec. V E. However, the vector polarization is small at all fields regardless of the length of the decay path.

If, instead of quenching the metastable atoms in a uniform magnetic field, we allow the beam to pass through a cylindrical quadrupole or hexapole magnet so that those atoms with positive magnetic moments are deflected out of the beam by the field gradient, a large enhancement of the nuclear vector polarization is obtained. Figure 15 shows the results of a calculation similar to that of Eq. (39), but with the summation restricted to those states j with magnetic moment $\mu_j = \partial E_j/\partial H \leq 0$. Table VIII

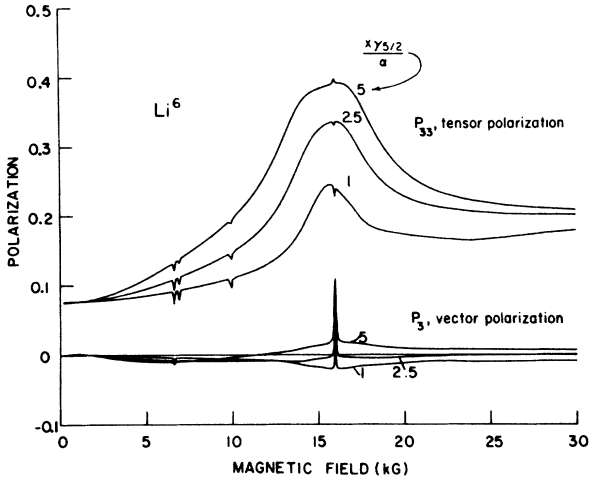

FIG. 14. Nuclear polarization in a beam of metastable Li^6 atoms as a function of magnetic field for various distances from the source.

summarizes the results for several values of the quenching-magnet length. In all cases, it is assumed that a suitable geometrical configuration exists to effect the complete separation of atomic magnetic moments. Hence, for magnets of 2.5, 5, and 10 decay lengths, vector polarizations of 70%, 90%, and 99% are obtainable with tensor polarization such that the beam is almost a pure "spin-1 down" beam.

The cost of this high vector polarization is, as usual, intensity, as can be seen from the last column of Table VIII. A figure of merit widely used in describing polarized ion sources[29] is the product P^2I, where P is the polarization and I the beam current. Figure 16 shows P^2I/I_0 as a function of H for both P_3 and P_{33}. Here I_0 is the beam current at the source of excitation. In this and the previous calculations, we have assumed that all metastable atoms remaining at some distance x from the source will auto-ionize and that the resultant ions can be collected and focused into an accelerator. Polarized

TABLE VII. Clebsch-Gordan coefficients for calculating nuclear polarization.

	$C^{J,1,J+1,M_F}_{J,(M_F-M_I),1,M_I}$	$C^{J,1,J,M_F}_{J,(M_F-M_I),1,M_I}$	$C^{J,1,J-1,M_F}_{J,(M_F-M_I),1,M_I}$
$M_I = 1$	$\left(\frac{(J+M_F)(J+M_F+1)}{(2J+2)(2J+1)}\right)^{1/2}$	$(-)\left(\frac{2(J+M_F)(J-M_F+1)}{2J(2J+2)}\right)^{1/2}$	$\left(\frac{(J-M_F)(J-M_F+1)}{2J(2J+1)}\right)^{1/2}$
$M_I = -1$	$\left(\frac{(J-M_F)(J-M_F+1)}{(2J+1)(2J+2)}\right)^{1/2}$	$\left(\frac{2(J-M_F)(J+M_F+1)}{2J(2J+2)}\right)^{1/2}$	$\left(\frac{(J+M_F)(J+M_F+1)}{2J(2J+1)}\right)^{1/2}$
$M_I = 0$	$\left(\frac{2(J-M_F+1)(J+M_F+1)}{(2J+1)(2J+2)}\right)^{1/2}$	$M_F\left(\frac{1}{J(J+1)}\right)^{1/2}$	$(-)\left(\frac{(J+M_F)(J-M_F)}{2J(2J+1)}\right)^{1/2}$

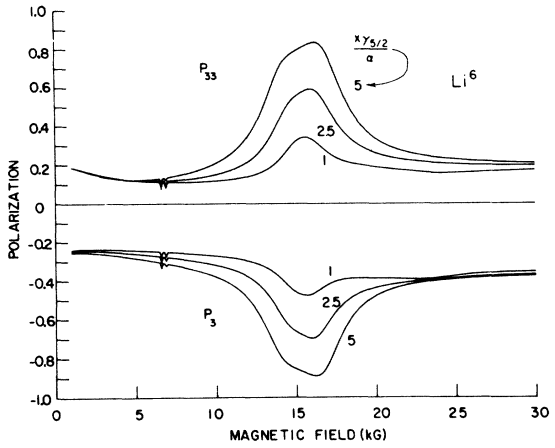

FIG. 15. Nuclear polarization as a function of field and distance from the source, calculated for an ensemble containing only negative magnetic moments.

Li^+ sources produced by the usual means of atomic-state separation followed by electron-impact ionization have recently been described by Ebinghaus *et al.*[30] and Miers and Anderson.[31] The calculated vector and tensor polarizations for Li^6 are $(32 \pm 1)\%$ and $(-32 \pm 1)\%$, respectively, while a beam current of 3.3×10^{-8} A was obtained experimentally.[31] Comparing the figure of merit $P_3^2 I$ for our hypothetical source to that for a conventional Li^6 source, we find the ratio

$$r = \frac{P_3^2 I/I_0}{(0.32)^2} \frac{\sigma(^4P)}{\sigma_I} , \tag{42}$$

where $\sigma(^4P)$ and σ_I are the maximum cross sections for excitation to the ^4P state and ionization, respectively. Since we obtain $\sigma(^4P)/\sigma_I \approx 10^{-3}$, then for $a = 1$ the ratio of figures of merit is about 10^{-4}. For larger values of a and higher resultant polarization, the ratio is even smaller, so that a practical source based on the differential metastability does not seem inherently feasible.

One possible means for increasing the intensity of the polarized beam is to selectively quench one of the long-lived substates in a radio-frequency field placed very close to the electron-bombardment source. In this way, we would collect mainly the auto-ionization products of a single sublevel before appreciable natural decay of that level. The polarization could reach 100% while the intensity might be perhaps 10% of the total metastable-beam intensity. While still not competitive with the conventional Li^6 source because of the small excitation cross section, this method promises significant improvement over the intensities given in Table VII.

The conclusion for He^3 is not necessarily the same. Since negative helium ions are believed to exist only in the $(1s2s2p)^4P$ state, there is no need for electron excitation, since microamperes of He^- are readily produced by commercially available charge-exchange sources. Blau *et al.*[32] observed differential metastability and Zeeman quenching in the decay of a He^- beam, and hence, state selection is also expected to occur. In principle, a calculation similar to the above can be performed. It is possible that a He^- source for a tandem Van de Graaff machine could be converted into a polarized ion source by the simple addition of a quenching magnet and the use of He^3 nuclei.

TABLE VIII. Polarization and intensity of a metastable Li^6 beam as a function of the number of decay lengths $a = x\gamma/\alpha$.

		Maximum polarization		
a	H(kG)	P_3	P_{33}	I/I_0
1	15.6	−0.476	0.341	3.37×10^{-2}
2.5	15.9	−0.697	0.590	5.58×10^{-3}
5	16.2	−0.891	0.835	7.10×10^{-4}
10	16.4	−0.983	0.970	3.48×10^{-5}
20	16.6	−0.999	0.998	2.94×10^{-7}

VII. CONCLUSION

The present results indicate that for quantities determined by the spin-spin interaction, such as $\gamma_{5/2}$ and c_{SS}, there is relatively good agreement between theory and experiment, while for quantities dependent on the spin-orbit and spin-other-orbit interactions, c_{SO}, $\gamma_{3/2}$, and $\gamma_{1/2}$, there are marked discrepancies. A survey of calculations[21] on the

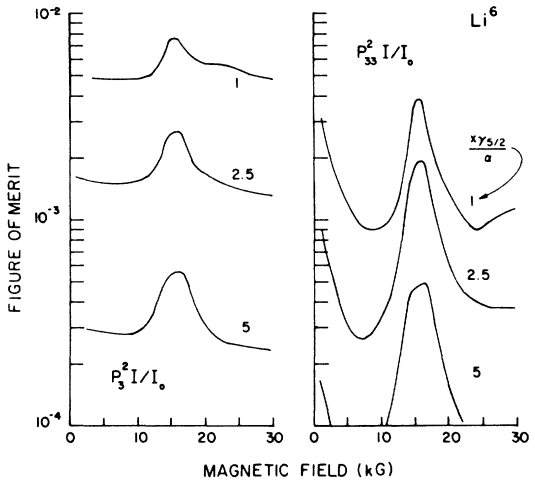

FIG. 16. Figure of merit of nuclear polarization as a function of field and distance from the source.

$(1s2p)^3P$ state of He also indicates that theoretical values of c_{ss} are more accurate than those for c_{so}, especially when correlation effects are neglected. It is suggested that these results reflect the fact that the spin-spin energy depends only on the electron wave functions, while the spin-orbit and spin-other-orbit energies depend not only on the wave functions for the electrons of interest, but, in addition, depend explicitly on the form of the atomic potential.

It will be necessary to develop precise three-electron wave functions in order to use improved measurements of the ^4P energy splittings as a test of the theory of the fine structure of simple atomic systems. It is hoped that the small natural linewidths of the metastable states will permit the measurement of the fs splittings to better than 1 ppm in an atomic-beam microwave-resonance experiment. The preliminary results[33] of such an experiment indicate that linewidths can be obtained which are about a factor of 10^2 narrower than anticrossing widths discussed in the present paper. This work may also improve the experimental value of $\gamma_{1/2}$ and $\gamma_{3/2}$.

The present results also indicate that the quenching of metastable atoms in a magnetic field (which focuses only atoms with negative magnetic moment) can result in nuclear polarizations which are larger than those obtained through conventional state-selection techniques. This may prove to be important for the development of a future source of polarized He^3 nuclei.

---

*Work supported wholly by the Joint Services Electronics Program (U. S. Army, U. S. Navy, and U. S. Air Force), under Contract No. DAAB07-69-C-0383.

†Alfred P. Sloan Research Fellow.

[1]P. Feldman and R. Novick, Phys. Rev. 160, 143 (1967).

[2]P. Feldman, M. Levitt, S. Manson, R. Novick, and G. Sprott, Physica 33, 278 (1967).

[3]P. Feldman (unpublished).

[4]P. Feldman, M. Levitt, and R. Novick, Phys. Rev. Letters 21, 331 (1968).

[5]M. Levitt and P. D. Feldman, Phys. Rev. 180, 48 (1969).

[6]G. Herzberg and H. R. Moore, Can J. Phys. 37, 1293 (1959).

[7]E. Holøien and S. Geltman, Phys. Rev. 153, 81 (1967).

[8]R. Novick and G. Sprott, Phys. Rev. Letters 21, 336 (1968).

[9]S. T. Manson, Phys. Rev. 145, 35 (1966).

[10]J. von Neumann and E. Wigner, Z. Physik 30, 467 (1929).

[11]S. T. Manson, Phys. Rev. A 3, 147 (1971).

[12]V. V. Balashov, V. S. Senashenko, and B. Tekou, Phys. Letters 25A, 487 (1967).

[13]Another case (excluding solids) in which an applied magnetic field has been observed to quench an excited state is that of the field-induced predissociation of the I_2 molecule. This effect is monitored by the quenching of the I_2 fluorescence at 18 500 cm^{-1} when a field 10–20 kG is applied. [Peter Pringsheim, *Fluorescence and Phosphorescence* (Interscience, New York, 1949), p. 199.]

[14]G. Herzberg, *Atomic Spectra and Atomic Structure* (Dover, New York, 1944), p. 156.

[15]A. Temkin, in *Autoionization*, edited by A. Temkin (Mono Book, Baltimore, 1966), p. 63.

[16]U. Fano, Phys. Rev. 124, 1866 (1961).

[17]B. R. Judd, *Operator Techniques in Atomic Spectroscopy* (McGraw-Hill, New York, 1963), p. 91.

[18]H. Kopfermann, *Nuclear Moments* (Academic, New York, 1958).

[19]D. A. Goodings, Phys. Rev. 123, 1706 (1961).

[20]K. C. Brog, T. G. Eck, and H. Wieder, Phys. Rev. 153, 91 (1967).

[21]References to experimental and theoretical work on He 2^3P can be found in F. M. J. Pichanick, R. D. Swift, C. E. Johnson, and V. W. Hughes, Phys. Rev. 169, 55 (1968). See also W. E. Lamb, Jr., *ibid.* 105, 559 (1957).

[22]H. A. Bethe and E. E. Salpeter, *Quantum Mechanics of One and Two-Electron Atoms* (Springer-Verlag, Berlin, 1957), p. 185.

[23]Ref. 22, p. 289. See also Appendix II in W. E. Lamb and R. C. Retherford, Phys. Rev. 79, 549 (1950).

[24]J. C. Pearl, D. P. Donnelly, and J. C. Zorn, Phys. Letters 30A, 195 (1969).

[25]I. S. Dmitriev, V. S. Nikolaev, and Ya. A. Teplova, Phys. Letters 26A, 122 (1968).

[26]R. J. Parker and R. J. Studders, *Permanent Magnets, and Their Application* (Wiley, New York, 1962), p. 188.

[27]I. C. Percival and M. J. Seaton, Trans. Roy Soc. (London) A251, 113 (1958).

[28]P. Feldman and R. Novick, in *Comptes Rendus du Congrès International de Physique Nucléaire*, Paris, 1964, edited by P. Gugenberger (CNRS, Paris, 1964), Vol. II, 4a/C144, pp. 785–786.

[29]J. M. Dickson, Progr. Nucl. Tech. Instr. 1, 105 (1964).

[30]H. Ebinghaus, U. Holm, H. V. Klapdor, and N. Neuert, Z. Physik 199, 68 (1967).

[31]R. E. Miers and L. W. Anderson, Rev. Sci. Instr. 39, 336 (1968).

[32]L. Blau, R. Novick, and D. Weinflash, Phys. Rev. Letters 24, 1268 (1970).

[33]M. Levitt, R. Novick, and S. Skwire, Bull. Am. Phys. Soc. 14, 943 (1969).